Journal of Arid Environments 75 (2011) 926–935

Contents lists available at ScienceDirect

Journal of Arid Environments

journal homepage: www.elsevier.com/locate/jaridenv

Surface energy and water vapor fluxes observed in a desert plantation in central Iran

A. Oliphant [a,*], P. Zawar-reza [b], G. Azizi [c], A. Dehghanpour [d], J. Harrison [b]

[a] Department of Geography, San Francisco State University, 1600 Holloway Avenue, San Francisco, CA 94132, USA
[b] University of Canterbury, Department of Geography, New Zealand
[c] University of Tehran, Department of Physical Geography, Iran
[d] Payam-e-noor University, Department of Geography, Iran

ARTICLE INFO

Article history:
Received 1 July 2010
Received in revised form
25 February 2011
Accepted 25 March 2011
Available online 24 May 2011

Keywords:
Surface radiation budget
Surface energy balance
Microclimate
Desert greening
Evapotranspiration
Local winds

ABSTRACT

Summertime observations of surface radiation budget, energy balance and atmospheric surface layer meteorology were made on an arid valley floor planted with *Haloxylon aphyllum* to combat desertification in central Iran. The surface microclimate is characterized and compared with other arid regions and the role of 'desert greening' on surface fluxes is considered. A high surface albedo (0.265) and large longwave radiation loss produced relatively low net radiation. Energy partitioning was dominated by sensible and ground heat fluxes with opposing diurnal asymmetry governed by strong diurnal variability in eddy diffusivity. The Bowen ratio was 2.53, which fell inside the range of other vegetated arid surfaces. Surface temperature gradients were strong both in the atmospheric surface layer and in the substrate, with consistent lapse conditions by day and inversions at night. The wind regime included a moderate daytime regional wind which displayed Coriolis turning and weaker nocturnal slope flows. Actual evapotranspiration (1 mm dy^{-1}) was only a small fraction of potential evapotranspiration. The diurnal pattern of AET indicates strong stomatal control. The desert greening effect of *Haloxylon* plantations provided atmospheric water and reduced sensible heat flux by up to 40%.

1. Introduction

Arid and semi-arid landscapes cover approximately one third of Earth's surface and provide an extreme thermal and hydrological boundary to the atmosphere. Despite such challenges for life, they provide habitat for a wide range of flora and fauna including more than one-fifth of the world's human population. Much of this population lives at the edge of agricultural sustainability where anthropogenic pressure can lead to severe land degradation, estimated to be currently present on 10–20% of the global dryland area (Reynolds et al., 2007). Furthermore, increases in aridity of many tropical and subtropical regions over this century are predicted due to anthropogenic global climate change (IPCC, 2007).

Understanding desert microclimates, especially exchanges of radiation, heat and water between the surface and atmosphere is critical for parameterization of surface schemes in global climate models as well as regional and forecasting models for improved climate and weather predictions. Despite their extensive global coverage and diversity of surface characteristics, arid environments have received relatively little observational attention to underpin parameterization of surface schemes. To date most observations of surface microclimates in arid environments have taken place in Australia (e.g. Cleugh and Roberts, 1994; Beringer and Tapper, 2000; Sturman and McGowan, 2009), North America, (e.g. Vehrencamp, 1952; Malek and Bingham, 1997; Kustas et al., 2000; Prater and DeLucia, 2006) and South America, especially Chile (e.g. Kampf et al., 2005; Kalthoff et al., 2006). Particularly little observational evidence exists of Middle Eastern arid environments, with the main exception being Israel (e.g. Heusinkveld et al., 2004).

This paper presents the first microclimate observations from Iran, focusing on a dune stabilization site near Yazd in an arid region of central Iran. The objectives of the study are to characterize the summertime surface radiation budget, energy balance and atmospheric surface layer meteorology, to compare these with observations from other arid environments, to examine the role of vegetation planted for dune stabilization on the water vapor flux and to test the use of existing empirical energy balance models in this environment. While a few studies have focused on microclimates of areas threatened by desertification (Grunwald et al., 1996) or microclimate impacts of non-native invasive species in semi-arid environments (Prater and DeLucia, 2006), we are not aware of any studies that investigate microclimates of 'desert greening' environments.

* Corresponding author. Tel.: +1 415 405 2143; fax: +1 415 338 6243.
E-mail address: andrewo@sfsu.edu (A. Oliphant).

0140-1963/$ – see front matter © 2011 Elsevier Ltd. All rights reserved.
doi:10.1016/j.jaridenv.2011.03.011

The surface energy balance of a vegetated surface is conveniently expressed in terms of the energy transfer into and out of a control volume including the vegetation, the canopy-air space and a layer of substrate deep enough to exclude heat transfer through its bottom, following (Oke, 1987):

$$Q_N = Q_H + Q_E + \Delta Q_S + Q_A \quad (1)$$

where Q_N is net all-wave radiation through the top of the volume, Q_H is sensible heat flux, Q_E is latent heat flux (both turbulent fluxes through the top of the volume), Q_A is the advective heat flux through all sides of the volume and ΔQ_S is the storage heat flux within the volume. Q_N is made up of the balance of four radiation components in two wavelength bands;

$$Q_N = K_N + L_N = K\downarrow - K\uparrow + L\downarrow - L\uparrow \quad (2)$$

where K is shortwave or solar radiation and L is longwave or thermal infrared radiation, the arrows indicate the direction of radiative flux relative to the surface and N refers to net exchange at the surface for a given wavelength band.

Q_A is neglected in many energy balance studies by siting instruments with a sufficiently homogenous and expansive upwind fetch so as to assume that horizontal exchanges of energy are negligible. Methods, definitions and assumptions used to determine ΔQ_S have varied widely but McCaughey and Saxton (1988) defined it comprehensively as:

$$\Delta Q_S = Q_G + Q_a + Q_w + Q_v + Q_p \quad (3)$$

where Q_G is the soil heat storage flux, Q_a and Q_w are the sensible and latent heat storage fluxes in the air-column below the turbulent flux measurement height, Q_v is the biomass heat storage flux, and Q_p is the photosynthetic heat storage flux. Energy balance studies in arid environments tend to neglect the last four terms since biomass is typically low and measurements are made sufficiently close to the surface so as to assume storage changes in the air volume are negligible (e.g. Beringer and Tapper, 2000). Even in large, densely vegetated forests Q_P was estimated to be extremely small (Oliphant et al., 2004). This leaves Q_H, Q_E and Q_G as the principal energy terms partitioned from Q_N in arid environments assuming adequate spatial homogeneity to neglect advection.

Characteristics of the radiation budget in arid environments include high $K\downarrow$ relative to the latitude of the location due to predominantly clear skies, high albedo (α) due to limited vegetation cover, low soil moisture and high sand concentrations and large thermal infrared radiation loss from the surface ($L\uparrow$) due to high surface temperatures of bare ground. As a consequence of these relatively high outgoing radiation terms, Q_N tends to be smaller relative to the magnitude of $K\downarrow$ compared with humid, vegetated surfaces (e.g. Malek and Bingham, 1997; Sturman and McGowan, 2009).

Table 1 presents a comparison of normalized energy balance partitioning reported in previous observational studies over a variety of arid and semi-arid surfaces. First, this comparison indicates that the partitioning of Q_N is commonly dominated by Q_H and Q_G. With limited or no vegetation and soil water, Q_E is usually a small term, often negligible. Further, the highest Q_E terms in this comparison exist where vegetation is present, indicating the importance of vegetation in the hydrologic cycle of arid environments and its role as a feedback mechanism in desertification or desert greening. Second, Table 1 indicates that very large variability exists between microclimates in different arid regions and even over small spatial scales within a region (e.g. Kampf et al., 2005) due to diversity of arid surfaces. This means that surface scheme parameterizations derived from one arid region cannot be accurately generalized for all arid regions. It is important to note that the relative magnitude of Q_G depends on the timing and length of period of observation which varies significantly in the studies synthesized in Table 1, which range from a few days to more than one year. Long term studies have shown that Q_G tends toward zero in sum over the annual cycle (Malek and Bingham, 1997; Oliphant et al., 2004).

Another common finding of energy balance components in arid areas is diurnal asymmetry in the relative magnitudes of the two dominant energy balance terms (Q_H and Q_G), where Q_G tends to peak mid-morning to mid-day and Q_H tends to peak mid afternoon (e.g. Cleugh and Roberts, 1994; Beringer and Tapper, 2000; Oliphant, 2000; Oliphant et al., 2007; Sturman and McGowan, 2009). This is because the thermal diffusivities of the two terms are driven by different processes. The transport mechanism for Q_G is thermal conductivity through the substrate material, which changes little over time (unless soil moisture changes or soil disturbance occurs). The transport mechanism for Q_H is eddy diffusivity which is dependent on the magnitude of turbulence near the surface. Since wind speed and turbulence typically peak in mid afternoon, energy is more effectively removed from the surface as Q_H relative to earlier in the day, leaving Q_G to peak earlier (Oke, 1987).

The closing of the surface energy balance (SEB) is a theoretical requirement of the first law of thermodynamics. Failure of observations to close the energy balance is typical and points to insufficiencies in the experimental set-up, the sensors, or to incomplete measurement of all energy flux terms. Several researchers have suggested lack of closure to be a problem of instrumentation, especially the underestimation of fluxes by the eddy covariance approach (Wilson et al., 2002; Oliphant et al., 2004). However, Foken (2008) suggested it was related to exchange processes operating on different scales within heterogeneous landscapes. Most of the studies in Table 1 reported a lack of energy balance closure, although these tended to be small (<10%) compared with more densely vegetated surfaces (see Wilson et al. (2002) for a useful comparison of SEB closure between different vegetation types). Most of the studies in Table 1 used the eddy covariance measurement approach but only about half of them had homogeneous surfaces. Compared with humid environments, the Q_G term shows very high diurnal amplitude in arid environments and therefore its measurement is relatively more important to SEB closure. Both Cleugh and Roberts (1994) and Heusinkveld et al. (2004) found different techniques to measure Q_G had a large impact on SEB closure over uniform surfaces and Kustas et al. (2000) found considerable spatial variability in Q_G in a Mesquite dune site due to variability in shading by foliage in patchy vegetation and microtopography, both common features of arid and semi-arid landscapes.

2. Physical setting and methods

The study site was located on the floor of a large arid valley about 20 km north of the city of Yazd near the geographic center of Iran (Fig. 1). The area lies on the western edge of the Dasht-e Lut and southern edge of the Dasht-e Kavir, Iran's two largest salt deserts which cover a combined area of about 100,000 km^2. The Yazd valley is oriented NNW–SSE and the floor is approximately 1200 m above sea level. Valley sidewalls rise ~1000 m above the valley floor to the east about 20 km away and ~1600 m to the west, about 30 km away. These ridges are branches of the broader Zagros Mountain Range to the west and are dominated locally by Shir Kuh, a 4050 m peak on the western ridge. The measurement site is a flat valley floor, comprised of fine sand with dune microtopography of 1–2 m. In order to protect irrigated agriculture and a city of half a million inhabitants (Yazd) from encroachment of sand from the

Table 1
Energy balance partitioning found in previous observational studies in arid and semi-arid environments.

Source	Location and site description	Q_H/Q_N	Q_E/Q_N	Q_G/Q_N	β
Sturman and McGowan (2009)	Clay pan, east-central Australia	0.56	0.11	0.08	5.02
Malek et al. (1990)	Playa, Great Salt Lake Desert, Utah, USA	0.73	0.30	0.02	2.5
	Vegetated playa margin, Great Salt Lake Desert, Utah, USA	0.28	0.67	0.049	0.43
Laymon and Quattrochi (2004)	Goshute Valley, Great Basin Desert, Nevada, USA	0.69	0.21	−0.23	3.43
Kampf et al. (2005) [a]	Salar de Atacama, Chile: Rough Halites (4 sites)	0.34–0.66	0.001–0.019	0.59–0.66	17.5–100
	Salar de Atacama, Chile: Border crusts (4 sites)	0.23–0.5	0.02–0.31	0.4–0.71	0.75–22
	Salar de Atacama, Chile: Vegetated surface (2 sites)	0.3–0.54	0.19–0.38	0.31–0.33	0.8–2.8
Cleugh and Roberts (1994)	Sparsely vegetated desert, central Australia	0.77	0.18	−0.03	−25
Oliphant (2000)	Sparsely vegetated intermountain basin, McKenzie Basin, New Zealand (2 sites)	0.78–0.79	0.16–0.17	0.05	4.6–4.9
Oliphant et al. (2007)	Frozen glacial till, Dry Valleys, Antarctica	0.43	0.21	0.10	2.02
Kalthoff et al. (2006)	Natural vegetation, Elqui valley, Norte Chico, Chile	0.60	0.035	0.19[b]	11
Beringer and Tapper (2000)	Sparse grassland, central Australia	0.75	~	0.25	∞
Malek and Bingham (1997)	Vegetated surface, Great basin desert, Nevada, USA	0.85	0.15	0	5.7

[a] Exact values not provided, estimates made from a bar graph of daily energy totals.
[b] Exact value not provided, calculated as a residual, since other terms and EB closure value provided.

north, the valley floor has been extensively planted with black saxaul (*Haloxylon aphyllum*). Saxaul is a woody C4 shrub with small leaves and a deep pivotal root system that thrives in dry, saline and sandy environments (Orlovsky and Birnbaum, 2002). It can be found growing naturally across most of arid Asia from Mongolia to the Caspian Sea and is used extensively for firewood, livestock grazing and to combat desertification (Orlovsky and Birnbaum, 2002). Biological methods to reduce desertification in Iran have been ongoing since 1959 and saxaul plantations cover some 20 million hectares of Iran, approximately 10% of this in Yazd Province (Baghestani Maybodi et al., 2006). Within the source area for micrometeorological measurements in this study, saxaul plants were 1–2 m high, 1–3 m in diameter and planted with 3 m spacing, producing a total surface cover of approximately 15–20%.

Mean monthly temperature in Yazd ranges from 5.1 °C in January to 32.4 °C in July, when mean monthly maximum temperature is almost 40 °C. Mean monthly diurnal temperature range changes little throughout the year and is approximately 14 °C. Mean annual precipitation total is 56 mm and most of this falls between December and May when it averages about 10 mm per month. The observations for this study were made in August and September, 2006.

Observations were made of the surface radiation budget, surface energy balance and meteorological profiles to 12 m using a pair of towers, 12 m and 3 m height separated by a distance of about 100 m. The surface radiation budget was measured at the top of the 3 m tower with a Q7 REBS net radiometer (REBS, Seattle, Washington), a pair of Li-200 pyranometers (LiCor Instruments Inc., Lincoln, Nebraska) facing upward and downward and an Everest4000 thermal infrared (TIR) radiometer facing the surface (Everest Interscience, Tucson, Arizona, USA). The field of view of downward pointing sensors was mostly sand with a little saxaul vegetation. The Q7 measured Q_N directly, and the bidirectional pyranometers measured $K\downarrow$ and $K\uparrow$ with albedo found from $\alpha = K\uparrow/K\downarrow$. As a means of comparison with solar radiation data observed at the surface, the equivalent extraterrestrial solar radiation flux (K_{ex}) was calculated for each 30-min period after Oliphant et al. (2003),

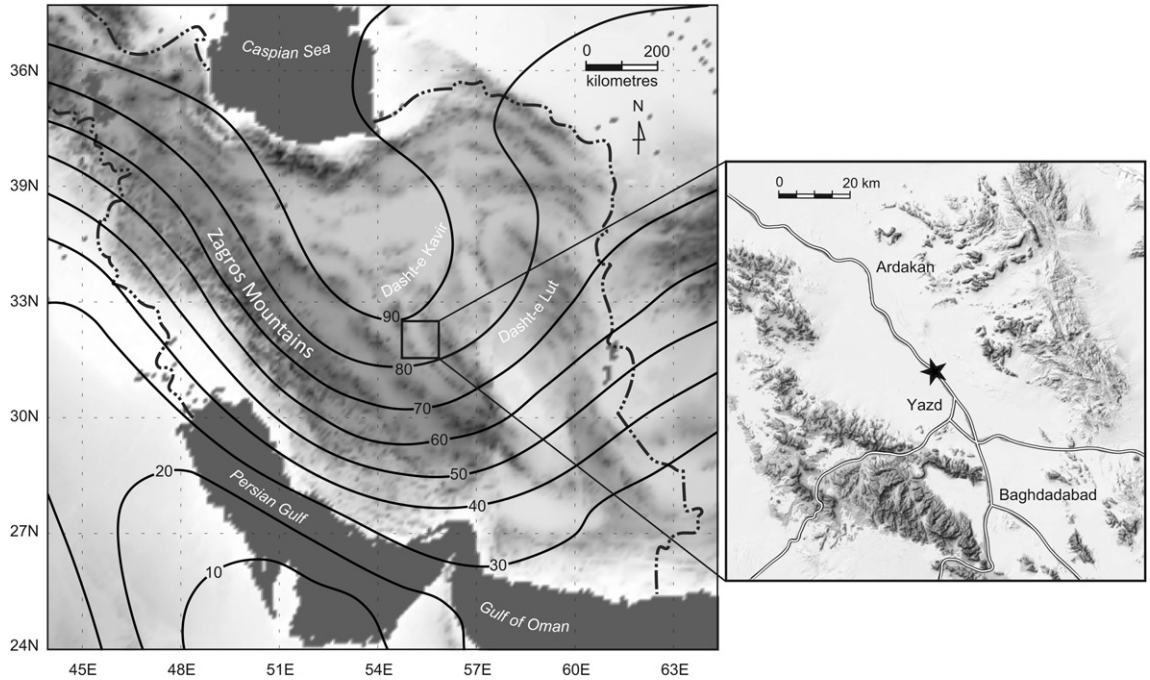

Fig. 1. Location maps for observational study site (indicated by a cross), located at N32.011232, E54.190045 near Yazd in central Iran. Green contour lines represent average geopotential height (m) at the 1000 hPa level during the period August 20th to September 3rd, 2006, based on NCEP reanalysis data.

$$K_{ex} = \left(I/r^2\right)\cos\theta \quad (4)$$

where I is the solar constant (1370 W m^{-2}), r is the ratio of the Earth-Sun distance to its mean, and θ is the solar zenith angle.

$$\cos\theta = \sin\Phi\sin\delta + \cos\Phi\cos\delta\cos h \quad (5)$$

where Φ is the latitude of the site, δ is the declination of the sun (ranging to 23.5° either side of the equator), and h is the hour angle of the sun from solar noon.

Unfortunately, the TIR radiometer ceased operating after only a few days of the experiment. However, salvaged data were used to perform a lag-dependent linear regression with sand temperature at 2 cm as the independent variable to estimate surface skin temperature (T_{surf}). The optimal model ($r^2 = 0.99$, $n = 452$) was found with a 100 min lag adjustment and was

$$T_{surf} = T_{S_2+100min} \times 1.64 - 25.1 \quad (6)$$

where $T_{S2+100\ min}$ is sand temperature measured by a T-type thermocouple at 2 cm at 100 min after the equivalent surface temperature. From surface temperature, the Stefan–Boltzman equation was used to derive $L\uparrow$ assuming an emissivity of 0.95 after Oke (1987). Net longwave (L_N) radiation was determined from $L_N = Q_N - K_N$ and $L\downarrow$ subsequently found by $L\downarrow = L_N - L\uparrow$.

For part of the study period the top of the tower cast a shadow over the upward pointing pyranometer for approximately 30 min during mid-morning (0930–1000 LST). $K\downarrow$ data from the period of local shading were removed and data were gap-filled using $K\downarrow = K\uparrow/\alpha$. Since α was very consistent during daylight hours (standard deviation was 0.01), this method was found to explain 99% of the variance in $K\downarrow$ by linear regression (slope = 0.265). In addition, since the sensor was completely shaded throughout one of the 10 min averaging periods (0940–0950 LST), it was assumed that the observed (shaded) $K\downarrow$ value for this period approximated the magnitude of diffuse beam solar radiation (K_D) and that $K\downarrow_{obs}/K\downarrow_{mod}$ for this period approximated the diffuse fraction of solar radiation (φ). This provided a daily mid-morning K_D and φ value for 16 days of the study period.

Eddy covariance measurements of turbulent heat fluxes (Q_H and Q_E) were made at 12 m with a CA27 one-dimensional sonic anemometer with fine wire thermocouple and a KH20 krypton hygrometer (Campbell Scientific Inc, Logan Utah). A second CA27 was deployed on the 3 m tower. The sampling frequency for the CA27 s and KH20 was 10 Hz with 30 min blocks for covariance calculations. A dry range (1.76–9.6 g m^{-3}) calibration coefficient was used for the KH20 and WPL and oxygen corrections were applied to the measurements in post processing (Campbell and Tanner, 1985; Leuning, 2004).

In calculating the ground heat storage term, as with previous observations in arid environments, we assumed the last four terms in Eq. (3) to be negligible and that $\Delta Q_S \approx Q_G$. Thus ΔQ_S, which will be more accurately termed Q_G henceforth, was determined using a REBS heat flow transducer (REBS, Seattle, Washington) buried at 4 cm depth in the fine sand substrate with a T-type thermocouple measuring sand temperature at 2 cm depth directly above the heat flow transducer. Q_G was then determined by

$$Q_G = Q_{G(z)} + C_S\frac{\Delta T_s}{\Delta t}z \quad (7)$$

where $Q_{G(z)}$ is the heat flow transducer buried at depth z (0.04 m), C_s is the heat capacity of dry sand and $\Delta T_s/\Delta t$ is the change in substrate temperature over the (1800 s) time period, measured by the thermocouple between the heat flow transducer and the surface. C_s was derived from $C_s = \rho_b\, c_{sd}$, where ρ_b is the bulk density of fine and dry sand and c_{sd} is the specific heat of dry sand. ρ_b values for dry sand tend to range from 1.5 to 2 Mg m^{-3} depending on sand grain dimensions and shape. In this case the sand was in the fine range of the spectrum so we used $\rho_b = 1.85$ Mg m^{-3} after Vepraskas (1988) and $c_{sd} = 890$ J kg^{-1} K^{-1} after Oke (1987). Heusinkveld et al. (2004) and Cleugh and Roberts (1994) found energy balance closure improved in two separate arid studies when heat flow transducers were buried at a very shallow depth (1–2 mm) and the heat storage term for the column above the transducer could be ignored. In this study, this was not advisable due to frequent wind disturbance of sediment which may have exposed part of the transducer to solar radiation, thereby contaminating the measurement. Unfortunately we only had one heat flow transducer available and the degree to which the single Q_G measurement site represented the source area of turbulent flux measurements is likely to add significant uncertainty to the ΔQ_S term. Because of the undulating surface microtopography and sparseness of vegetation, the most representative site for a single sensor was deemed to be on a horizontal surface within a clearing. This site selection may have resulted in overestimation of Q_G due to lack of shading by vegetation. Several past observational studies of Q_G have emphasized the need for multiple sampling sites to account for spatial heterogeneity (e.g. Kustas et al., 2000). Hence our single sampling site is a limitation of this study.

Air temperature, relative humidity (HMP45C, Vaisala, Helsinki, Finland) and wind speed (A101M-L cup anemometer, Vector Instruments, North Wales) were measured at 1, 3, and 12 m above the surface and wind direction was measured at 12 m (W200P wind vane, Vector Instruments, North Wales). Soil temperatures were measured at 2 and 10 cm depths in the dry, fine sand substrate using T-type thermocouples. Sampling frequency for radiation and meteorological variables was 1 s with a 10 min averaging period.

Data quality control was conducted by spike detection and plausible bound fitting algorithms as well as visual inspection and energy balance closure tests. The harsh environmental conditions in this study as well as access difficulties lead to significant data rejection, mostly due to periods of instrument failure. Wind direction was used to reject turbulent flux data from the south to southwest directions due to the presence of irrigated crops and urban surfaces within the suspected flux source area. However, most of the wind direction was from the north, east and west, where the surface was representative of our study objectives and the source area for Q_N and Q_G observations. Our broader analysis focuses on the period when most instruments were operational from August 9th (day of year (DOY) 222) to September 24th (DOY 268), 2006. Eddy covariance data were generally more limited both by instrument failure and several periods of southerly flow, so we focus more detailed analysis of the surface energy balance and associated radiation budgets and atmospheric surface layer meteorology on a 'golden' 15-day period from August 20th (DOY 233) to September 3rd (DOY 247).

3. Results and discussion

3.1. Meteorological conditions

Synoptic conditions during the observational period were typical for the location and season, being dominated by high pressure with strong subsidence and lack of clouds or precipitation. Average geopotential height contours for the 15-day period of detailed analysis (Fig. 1) reveal a consistent regional scale pressure gradient from the Caspian Sea in the north to the Persian Gulf and Gulf of Oman in the south. This is typical throughout the summer months producing prevailing northerly winds over much of

southern Iran (Hossenzadeh, 1997; Zawar-Reza, 2008). Conditions during the study period were consistently dry and warm with moderate to strong winds (Fig. 2). Mean temperature at 3 m for the period was 27.8 °C, mean daily maximum was 36.8 °C and mean daily minimum was 16.7 °C. Mean daily wind speed at 12 m was 2.8 m s^{-1} and mean daily maximum wind speed (10 min average) was 5.9 m s^{-1}. Relative humidity averaged 13.4% with the lowest recording being 3.9%. Near the end of the observational period, a weak disturbance passed through the study site which included the strongest winds (maximum for a 10 min average was 9.3 m s^{-1}) and produced significant cooling (daily average dropped 6.5 °C) and a smaller increase in humidity (peak daily average was 32%). In the following sections, we examine ensemble diurnal patterns and statistics derived from the detailed period of analysis (DOY 233–247).

During the period of detailed analysis, sunrise occurred at about 0530, sunset at 1830 and solar noon at 1200, all local standard time (LST = UTC + 3.5 h). Diurnal wind fields were very consistent by day with moderate to strong NNW flow and weaker and more variable flow at night from the east and west (Fig. 3). The daytime flow was initiated about 0900 LST (3.5 h after sunrise and 1.5 h after lapse conditions were established), peaked in strength at 1600–1700 LST and continued until about 1900 LST (shortly after sunset). The daytime flow appears to represent the regional scale pressure gradients and is potentially enhanced by a local-scale up valley thermal circulation. Throughout the day, a very slow but consistent directional veering to the right occurred, amounting to approximately 30° over a 12 h period. This suggests the circulation was sufficiently large and consistent to experience observable Coriolis forcing. Since the scale of valley wind circulations seldom produce observable Coriolis turning (e.g. Whiteman, 1990), this points to the dominance of the regional scale flow by day. Following sunset, the northerly daytime flow was replaced by a consistent ENE flow for about four hours with a secondary peak in wind speed

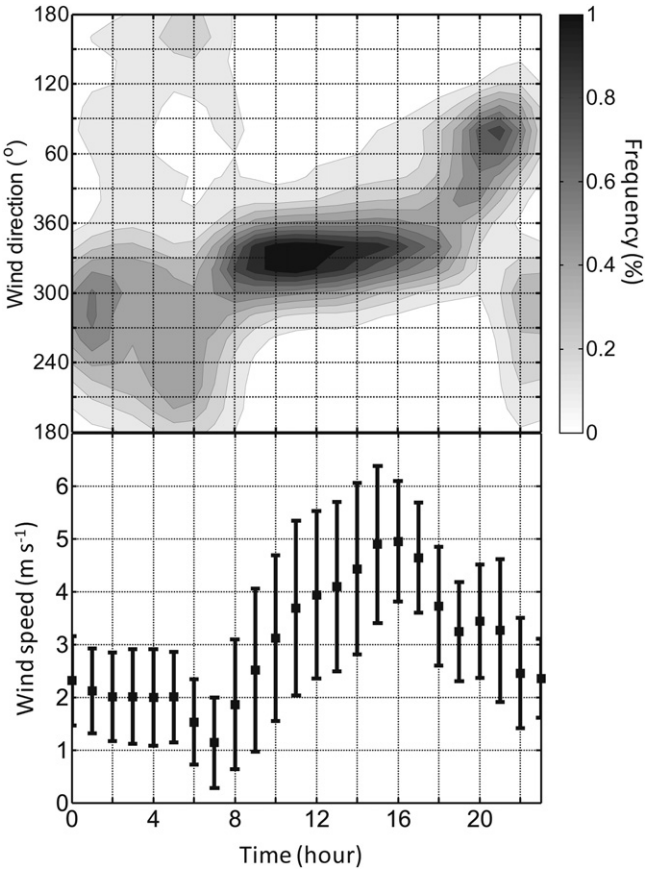

Fig. 3. Ensemble hourly wind direction frequency and average wind speed (solid squares) ± 1 standard deviation (error bars) at 12 m from DOY 233–247, 2006 in Yazd, Iran.

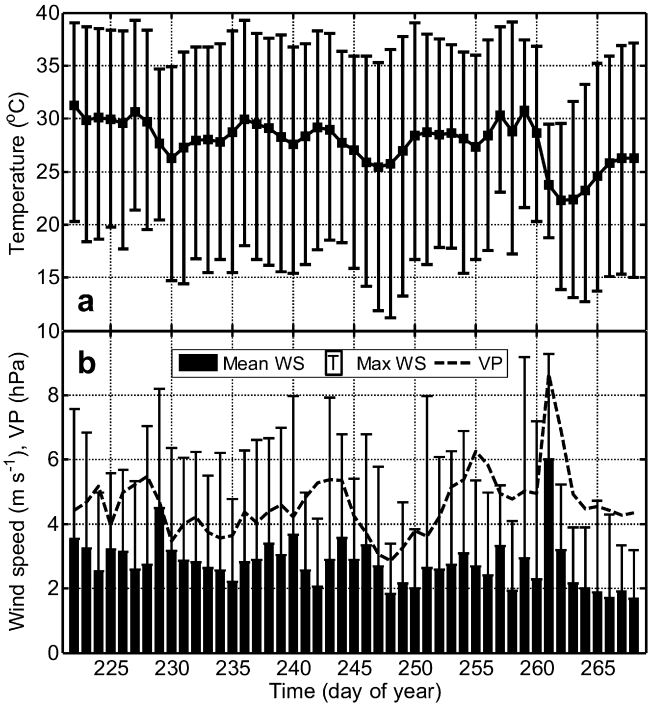

Fig. 2. (a) Daily mean, maximum and minimum temperatures at 3 m, (b) daily mean vapor pressure at 3 m and daily mean and maximum wind speed at 12 m. Data are based on 10 min averages from DOY 222–268, 2006 in Yazd, Iran.

about 2000 LST. The origin of this flow is uncertain. It is too strong to represent onset of a drainage flow but may result from localized channeling through a gap in the ENE valley sidewall (Fig. 1) of the regional flow which was veering eastward. From 2300 until the onset of the daytime flow, wind was relatively weak but predominantly from the west and with a strong surface inversion (Fig. 4a). This suggests the main nocturnal flows may be drainage flow from the dominant western valley sidewall. A SSE down-valley wind is not apparent in the nocturnal wind field. The diurnal minimum wind speed occurred quite abruptly around sunrise, probably reflecting the period when sunrise onto the western (east-facing) slope shut down the slope flow but valley heating was as yet insufficient to develop the valley wind or cause sufficient downward mixing of regional scale airflow. This type of morning transition has been shown previously in both observation and theory (e.g. Whiteman, 1990). Confirmation of the derivation of these wind fields will be investigated using mesoscale modeling.

Diurnal temperature gradients (between 1 and 12 m) show an inversion formed around sunset and lapse conditions were established by two hours after sunrise (Fig. 4a). The unstable atmospheric surface layer produced by the daytime lapse seemed to produce significant downward mixing of momentum, reflected by rapidly increasing wind speeds consistent to the 1 m level as the lapse strengthened in the morning hours (Fig. 4a and b). The early nocturnal easterly flow caused a peak in wind speed at all levels and the surface inversion was weakened during this period due to mixing. By midnight the westerly flow was established with a much stronger inversion which appeared to cause a relative decoupling in wind speed between the 3 and 12 m levels.

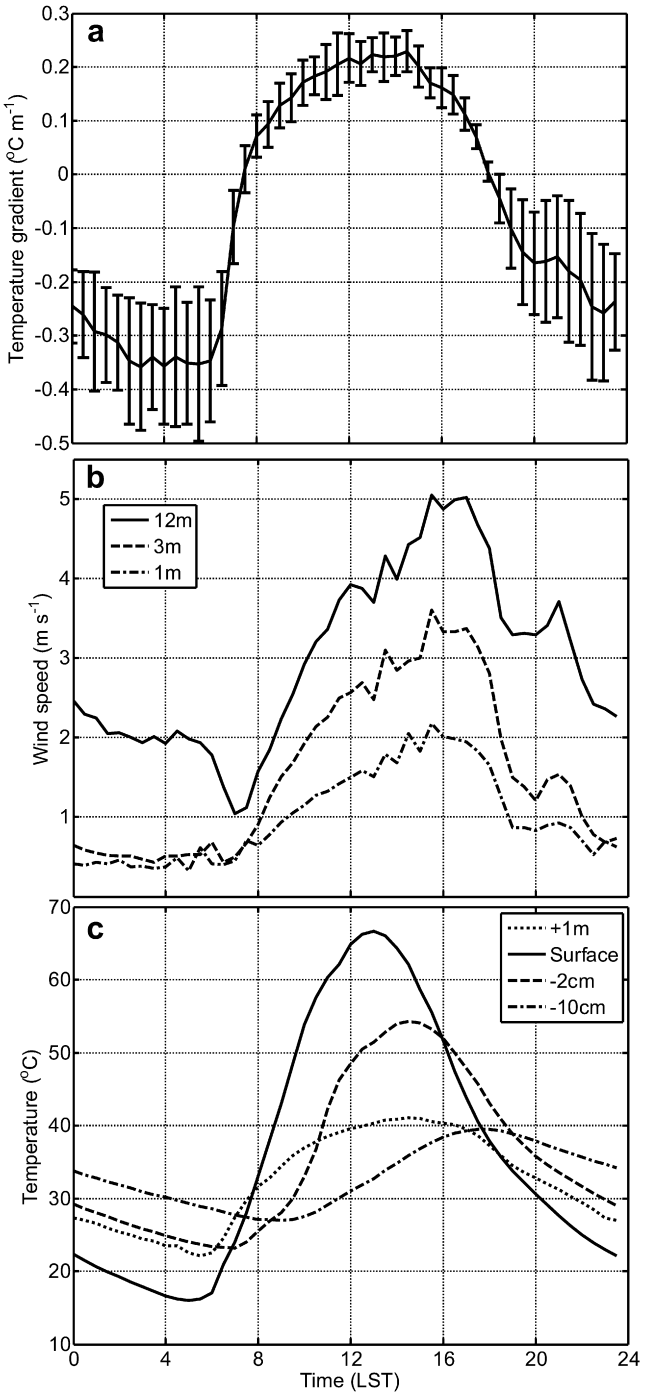

Fig. 4. Diurnal ensemble (a) average and standard deviation temperature gradient between 1 and 12 m, (b) average wind speed at three levels, (c) average temperatures at four levels in the substrate and overlying air. All data are 30 min ensembles from DOY 233–347, 2006 in Yazd, Iran.

The temperature gradient in the 10 cm beneath the surface was extreme, peaking at 3.2 °C cm^{-1} at solar noon (Fig. 4c) and −1.3 °C cm^{-1} shortly before sunrise (positive values implies a temperature increase away from the surface and vice versa). The diurnal temperature range was 50.6 °C at the surface, 31.1 °C at 2 cm and 12.5 °C at 10 cm. The lag time between temperature minima and maxima at the surface and 2 cm was 100 min and between the surface and 10 cm it was 310 min. This illustrates a considerable amount of heat storage in the shallow soil layers and an extreme microclimate for vegetation to adapt to. Air temperature at 1 m, had a diurnal range of 18 °C with its minimum just before sunrise and maximum at 1430 LST.

3.2. Surface radiation budget

Daily total radiation flux densities and 30 min ensemble averages during the period of analysis are provided in Table 2 and Fig. 5 respectively. The diurnal pattern of $K\downarrow$ closely followed that of K_{ex} and peaked near 1000 W m^{-2} at solar noon due to a lack of clouds during the study period and a low solar zenith angle (average = 19° at solar noon). The daily total $K\downarrow$ was 73% of K_{ex} and varied little through the study period (Table 2). Mid-morning diffuse fraction (φ) averaged 0.13 and also varied little. The relatively high attenuation (for clear skies) and low φ suggest significant atmospheric absorption which points to the presence of large aerosols such as dust entrained from the desert. Although not measured, this atmospheric dust was clearly apparent to the observer on the surface, especially near sunset. Mean daylight albedo (α) over the study period was 0.265 with negligible influence of solar angle and a daylight standard deviation of only 0.01. $L\downarrow$ has a strong diurnal signal, with a peak around the middle of the day. This daytime peak is higher than that calculated for clear skies using Sridhar and Elliot's (2002) modified Brutsaert (1975) down-welling longwave radiation equation, although the nocturnal $L\downarrow$, agrees well. A small portion of this difference is likely to be due to the additional input of down-welling longwave radiation emitted from the sidewalls of the valley, although the terrain view was a very small fraction of the sky view factor due to the width of the valley (terrain elevation angle <5°). Another likely contribution to this peak is the role of atmospheric aerosols on effective clear sky emissivity (ϵ). When calculated as a residual from the Stefan–Boltzman equation and observed $L\downarrow$, ϵ ranged from approximately 0.7 at night to 0.8 during the day. This is high in general for clear sky ϵ (e.g. Sridhar and Elliot, 2002) and, in addition to the large diurnal range, suggests significant control on $L\downarrow$ by atmospheric aerosols. $L\uparrow$ was extremely large due to high surface temperatures (Fig. 6), to the point that daily total $L\uparrow$ was greater than K_{ex} (Table 2). With clear nights, daily L_N loss was significant (52% of K_N). As a consequence of the high surface albedo and temperature and clear skies, the net losses of energy by radiation were large (83% of net incoming) and the resulting Q_N was small relative to solar radiation (35%). Low $Q_N/K\downarrow$ has been reported from a number of observations in arid environments (e.g. Malek and Bingham, 1997; Sturman and McGowan, 2009).

Throughout the operational period for radiation sensors, this pattern remained remarkably unchanged (Fig. 6). There was a steady seasonal decline in K_{ex} which was reflected closely in $K\downarrow$, due to largely unchanging sky conditions. $L\uparrow$ also declined at a similar rate, commensurate with surface absorption of solar radiation, although was clearly also affected by air temperature (compare with Fig. 2a). $L\downarrow$ remained more constant throughout the study period and was closely linked with air temperature (Fig. 2a).

Table 2
Daily statistics for radiation flux magnitudes and ratios from Yazd, Iran day 233–247.

Flux magnitudes	K_{ex}	$K\downarrow$	$K\uparrow$	K_N	$L\downarrow$	$L\uparrow$	L_N	Q_N
Average (MJ m^{-2} d^{-1})	36.3	26.3	6.94	19.4	28.8	38.9	−10.1	9.24
Std. dev (MJ m^{-2} d^{-1})	0.66	0.87	0.2	0.67	1.39	1.34	0.69	0.21
Flux ratios	α	$K\downarrow/K_{ex}$	Q↑/Q↓	φ[a]	L_n/K_n			
Average (ratio)	0.264	0.73	0.83	0.13	0.52			
Std. dev. (ratio)	0.002	0.02	0.006	0.03	0.20			

[a] Values from mid-morning only.

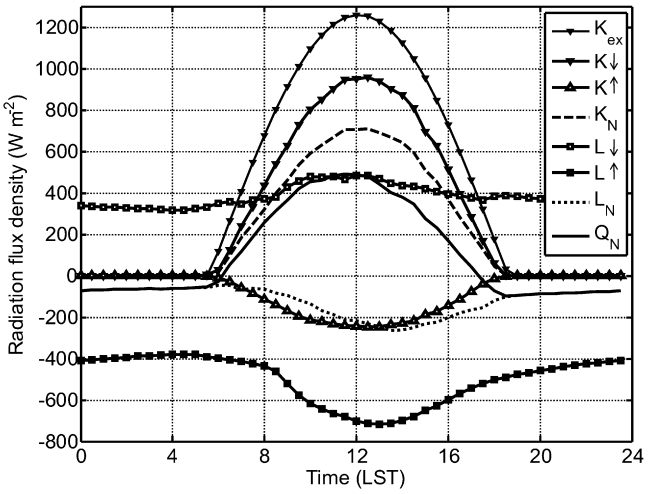

Fig. 5. 30 min ensemble average radiation fluxes for DOY 333–347, 2006 in Yazd, Iran.

3.3. Surface energy balance

Surface energy balance closure was assessed initially by examining the balance between radiation and ground heat fluxes (Q_N–Q_G) and turbulent heat fluxes ($Q_H + Q_E$) directly for all quality assured 30 min periods during the study (Fig. 7a). The overall agreement was good with a slope just below unity and a $-10\ W\ m^{-2}$ offset, suggesting the turbulent fluxes slightly under-estimated available energy from radiation and ground fluxes. The sign of this imbalance is common though the magnitude is smaller than most terrestrial surfaces (Wilson et al., 2002). However, relatively good energy balance closure has been found at other arid sites (e.g. Cleugh and Roberts, 1994; Beringer and Tapper, 2000; Oliphant, 2000; Kampf et al., 2005; Sturman and McGowan, 2009). The source area for turbulent flux measurements at 12 and 3 m above the surface are vastly different (source area at 12 m would be on the order of 50 times larger). Therefore it is interesting to compare the two identical CA27 instruments for Q_H measurement mounted at different heights (Fig. 7b). Overall, Q_H estimates from the two heights agree closely, with Q_H at 12 m explaining 98% of the variance of Q_H at 3 m. However, the site at 3 m is consistently higher by about 18% than at 12 m. From observation at the study site it seems likely that this difference was caused by a smaller density of vegetation within the much smaller footprint of the 3 m tower. Using the 3 m Q_H value or an average of the two heights reduces the energy balance closure compared with using the 12 m level. Therefore in further analysis we use the 12 m Q_H measurement. This comparison does suggest however that Q_H values reported in this study are more likely to be an under- than overestimation.

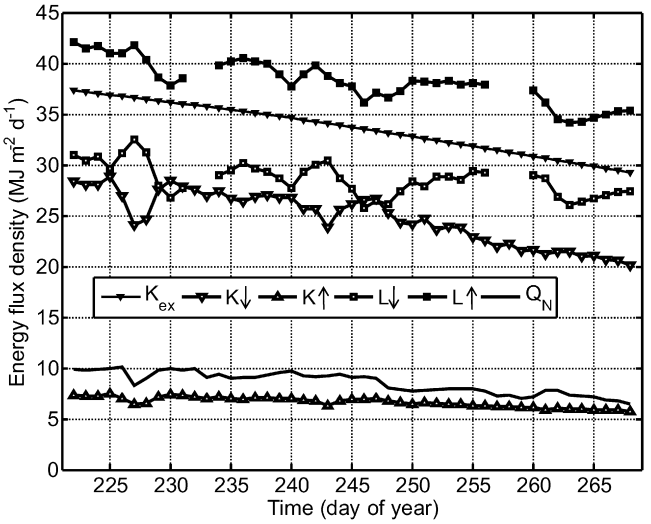

Fig. 6. Daily total radiation fluxes for DOY 222–268, 2006 in Yazd, Iran.

The close energy balance closure at this and other arid sites might reflect the lack of dense vegetation, relative homogeneity of surfaces, lack of significant latent heat fluxes and typically low measurement heights compared with humid (particularly forested) sites. In this case the strong turbulent condition due to high surface temperatures and strong winds reduces likely under-measurement in the eddy covariance method in low turbulence conditions (e.g. Wilson et al., 2002; Oliphant et al., 2004). This is suggested by the relative closeness of the data to the 1:1 line at high magnitudes during the day and the general underestimation of turbulent fluxes when Q_N–Q_G is between -50 and $20\ W\ m^{-2}$, reflecting weaker turbulent intensity under lower wind speed and stable stratification in the nocturnal atmospheric surface layer (Fig. 4a and b). A second region of underestimation of Q_N–Q_G by $Q_H + Q_E$ occurred when the former was between 200 and $300\ W\ m^{-2}$. From the diurnal pattern of the residual in the energy balance (Fig. 8), it can be seen that this reflects the mid-morning period when Q_G dominates energy partitioning. This could be due to the overestimation of Q_G by sampling in a clearing and underestimating surface shading by vegetation. However, the residual energy as a fraction of Q_N was less than 10% so closure analysis generally provides confidence for the robustness of energy balance magnitudes reported below.

Ensemble average diurnal energy balance fluxes for the study period show the dominance of Q_H and Q_G in partitioning net radiation (Fig. 8). There is strong asymmetry between their peaks with Q_G dominating the morning hours and Q_H the afternoon. Following sunrise, almost all available energy was driven by conduction into the substrate, at a time when wind speed was at its diurnal minimum (Fig. 4c). Q_G peaked mid-morning at a time when the substrate temperature gradient between the surface and 2 cm was strongest. By mid afternoon, Q_G turned negative, and the temperature gradient between the surface and 2 cm reversed, with net conductance back upward toward the surface.

Santanello and Friedl (2003) provided an empirical equation for daytime Q_G as a function of Q_N for a number of bare soil environments:

$$\frac{Q_G}{Q_N} = A\cos\left[\frac{(t+10800)}{B}\right] \tag{8}$$

where A represents the maximum daytime value of Q_G/Q_N, B is a time period in seconds (s) that adjusts the phase and t is time in seconds relative to solar noon. For a range of types of dry soils (<5% soil water content) Santanello and Friedl (2003) found A and B to be best represented by 0.35 and 100,000 s respectively. They also provided linear adjustments for A and B that could be found from the diurnal range of surface temperature (ΔT_{surf}), using $A = 0.0074\ \Delta T_{surf} + 0.088$ ($r^2 = 0.91$) and $B = 1729\ \Delta T_{surf} + 65013$ ($r^2 = 0.56$). For the current study, this produces $A = 0.46$ Q_G/Q_N and $B = 150{,}000$. The increase in A in drier soils is because less energy is utilized for evaporation and the increase in B reflects slower thermal conductivity in drier soils, shifting the phase of Q_G/Q_N slightly later in the day. The uncertainty difference between r^2 values in finding A and B using ΔT_{surf} suggests the phase timing is more difficult to predict than the overall magnitude of Q_G/Q_N. Applied to the data in this study, both the generalized dry soil

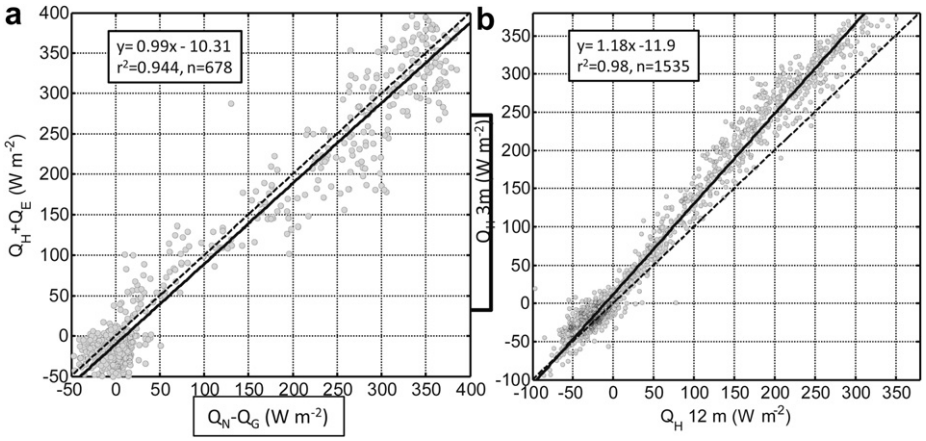

Fig. 7. (a) Energy balance closure for DOY 333–347 and (b) 3 vs 12 m Q_H for all good CA27 measurements during the period DOY 222–268, 2006 in Yazd, Iran.

parameterization and that found by ΔT_{surf} produced an under-prediction of Q_G (simulations 1 and 2, Table 3). The ΔT_{surf}-derived A (0.46) matched very closely to the observed maximum Q_G/Q_N and improved the magnitude of prediction. However, the phase observed at this site was rather earlier than the ΔT_{surf}-derived B (150,000 s) produced. Hence using the ΔT_{surf}-derived A while maintaining the initial recommended B value improved the Q_G prediction significantly (simulation 3, Table 3). A and B were also found by a best fit routine, which produced 0.56 and 85,000 respectively and the best model performance (simulation 4). Thus the magnitude of Q_G/Q_N was extremely high in this study as predicted for very dry soils but the phase was significantly earlier than predicted by the Santanello and Friedl (2003) equation. This seems to reflect the neglect in this scheme of the changing ratio of eddy diffusivity to thermal conductivity throughout the day. In this case, with strong afternoon winds and temperature gradients in the atmospheric surface layer, surface energy is much more effectively partitioned into Q_H, and Q_G becomes negligible by early afternoon.

In order to investigate the role of transport mechanisms in the asymmetry between Q_H and Q_G, we plotted the relation between wind speed and the ratio Q_H/Q_G which appeared positive but non-linear (Fig. 9). The relation takes a rectangular hyperbola form and the empirical parameters were found by best fit with the observational dataset when both Q_H and Q_G were positive ($r^2 = 0.48$, $n = 218$),

$$\frac{Q_H}{Q_G} = \frac{(\lambda R_{max} u)}{(R_{max} + \lambda u)} - c \quad (9)$$

where λ is the initial slope (1.8), R_{max} is the value of Q_H/Q_G when the relation saturates (3.1) and u is wind speed (m s^{-1}). This relation suggests there is a positive increase in Q_H/Q_G with wind speed, the slope of which decreases as wind speed increases. In this case, Q_H became larger than Q_G when wind speed was greater than 1.6 m s^{-1} (found by solving for wind speed when $Q_H/Q_G = 1$) and Q_H dominance saturated by the time Q_H was 3.1 times greater than Q_G. The relation was quite weak, which is not surprising since wind speed is only a proxy for the thermal conductivity difference between the atmosphere and substrate. In the late afternoon, Q_H briefly increased to slightly larger than Q_N, and it appears the additional energy was derived from a reversed Q_G, which supplied about 80 W m^{-2} to the surface at this time. Both this and the diurnal asymmetry between Q_H and Q_G reported here has been observed in a number of other arid environments (e.g. Cleugh and Roberts, 1994; Beringer and Tapper, 2000; Oliphant, 2000; Oliphant et al., 2005; Sturman and McGowan, 2009).

Over the diurnal cycle, Q_G summed to near zero (Table 4) because its significant daytime gain was offset by a roughly equivalent nocturnal loss. This is to be expected, as well as the slight negative Q_G total suggesting that on the seasonal timescale, ground temperatures were starting to cool. The remainder of energy was therefore partitioned between Q_H (~65%) and Q_E, (~27%) over the 24 h cycle. When considering just the daylight period, both turbulent heat flux fractions were smaller with Q_G being a larger fraction than Q_E. Energy balance partitioning in this study agrees closely with the broader picture of energy balance in arid environments (Table 1), including a Bowen ratio larger than unity, in this case

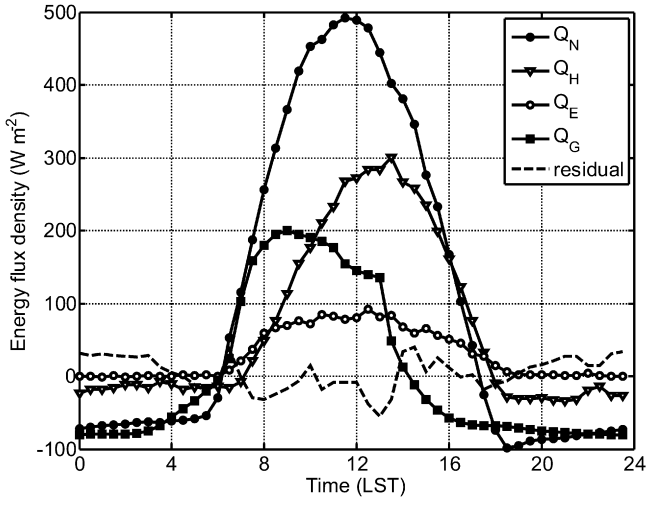

Fig. 8. 30-minute ensemble average energy balance fluxes and residual energy for DOY 333–347, 2006 in Yazd, Iran.

Table 3
Statistics for daytime Q_G predictions based on different parameters for the Santanello and Friedl (2003) scheme (Eq. (8)), where; RMSE = $\sqrt{\sum_{i=1}^{n}(P-O)^2/n}$; MAE = $\sum_{i=1}^{n}(|P-O|)/n$;MBE = $\sum_{i=1}^{n}(P-O)/n$; P is the predicted Q_G derived from Eq. (8) and observed Q_N and O is observed Q_G during the period of analysis.

Simulation	A	B	Slope	r^2	RMSE (W m^{-2})	MAE (W m^{-2})	MBE (W m^{-2})
1	0.35	100	0.56	0.83	53.4	46.9	−39.4
2	0.46	150	0.61	0.62	46.2	36.2	14.2
3	0.46	100	0.74	0.83	31.7	23.7	−9.53
4	0.56	85	0.99	0.83	32.9	26.9	−0.53

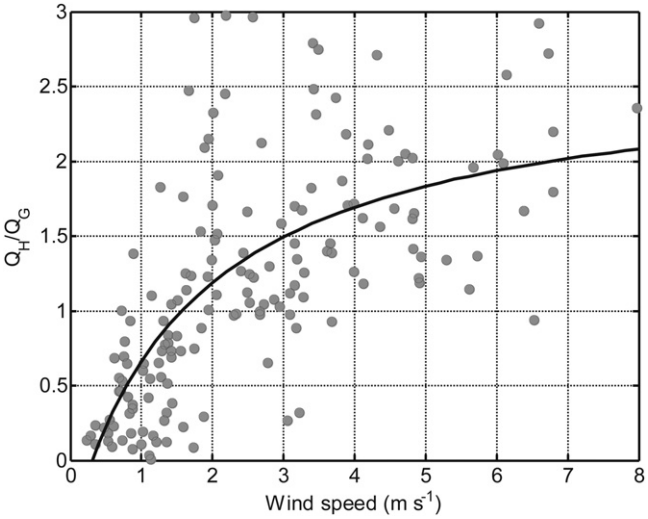

Fig. 9. Relation between wind speed and daytime Q_H/Q_G for 30 min periods when both Q_H and Q_G were positive (see Eq. (9) for definition), DOY 333–347, 2006 in Yazd, Iran.

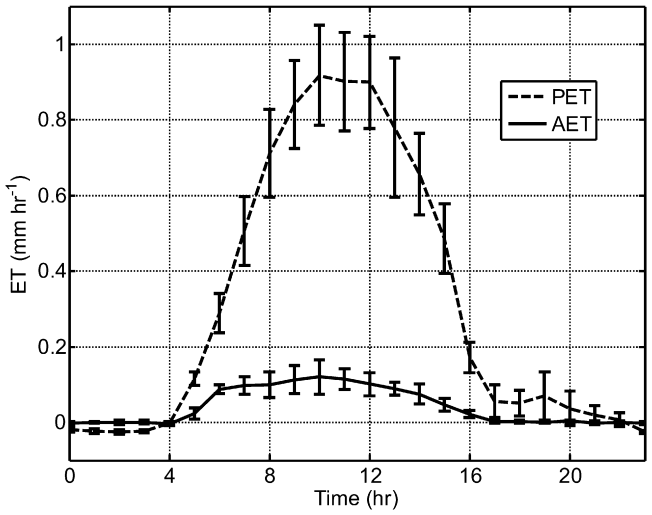

Fig. 10. Hourly ensemble average potential and actual evapotranspiration for DOY 333–347, 2006 in Yazd, Iran.

between 2.5 and 3. The 15 days making up the summary statistics presented very little variation in this partitioning (Table 4).

3.4. Water vapor flux

Q_E rose in mid-morning to about 80 W m^{-2}, where it seemed to plateau until early afternoon before diminishing steadily and reaching zero an hour before sunset (Fig. 8). The mass flux of actual evapotranspiration (AET) was determined from Q_E using temperature-dependent latent heat of vaporization ($AET = Q_E/L_{v(t)}$) and converted to mm (Fig. 10). The potential evapotranspiration (PET) was computed at hourly time steps from a modified Penman–Monteith equation using Jensen et al. (1990) and forcing surface resistance to 0, thereby examining just the atmospheric demand. AET reached a diurnal maximum of 0.12 mm h^{-1}, which was a small fraction of the atmospheric demand for moisture (Fig. 10). Daily total AET was 1.0 ± 0.34 mm dy^{-1}, which was only 13.5% of PET which was 7.4 ± 1.6 mm dy^{-1}. In fact, without surface resistance it would take only one week to evaporate the equivalent annual precipitation. The large difference between AET and PET therefore shows extremely high surface resistance. Although soil moisture near the surface was not measured, it could be assumed that it was negligible based on visual observations of the sand in the top 10 cm of the dunes. This means the principal evaporative flux was by transpiration from the saxaul plants which were able to draw moisture from deeper in the substrate using their extensive and deep root system (Orlovsky and Birnbaum, 2002). The initial jump in AET immediately following sunrise suggests some early photosynthetic activity by the plants with associated moisture loss. This is also the most consistent period of daylight hours through the study period (see standard deviation error bars in Fig. 10). The plateau, followed by the gentle decline shows that root level water was also scarce and canopy resistance was also high. Kobayashi et al. (2010) compared biological functioning of various arid shrublands and showed that *Haloxylon aphyllum* (black saxaul) had generally low stomatal conductance (0.02–0.04 mol m^{-2} s^{-1}). The diurnal pattern of stomatal conductance they presented closely follows the pattern in transpiration evident in Fig. 10, with a peak conductance in mid-morning and a general decline in the afternoon. They also showed strong correlation between soil moisture and stomatal conductance and leaf water potential and stomatal conductance. Hence the shrub is able to yield strong stomatal control to ensure survival during water stress and the results of this are evident in the diurnal transpiration pattern.

Although small, AET at this site does provide a measurable quantity of water to the atmosphere of 1 mm dy^{-1}. Thus, planting of saxaul for dune stabilization has an impact on the local microclimate, both by providing a source of atmospheric moisture and by reducing Q_H. If we assume that evaporation from the bare dune fields would be negligible based on lack of soil moisture, then the Bowen ratio at this site without saxaul plantation would tend toward infinity and Q_H would be approximately 2.5 MJ m^{-2} dy^{-1} (40%) greater. Thus the desert greening effects of saxaul plantations on the local microclimate are significant.

Table 4
Daily statistics for energy flux magnitudes and ratios from Yazd, Iran day 233–247.

Flux magnitudes (24 h)	Q_N	Q_H	Q_E	Q_G	Residual
Total (MJ m^{-2} d^{-1})	9.24	6.01	2.48	−0.11	0.88
St. dev. (MJ m^{-2} d^{-1})	0.21	0.63	0.43	0.51	0.69
Flux magnitudes (daytime)	Q_N	Q_H	Q_E	Q_G	Residual
Total (MJ m^{-2} d^{-1})	12.06	6.80	2.44	2.66	0.16
St. dev. (MJ m^{-2} d^{-1})	0.21	0.55	0.40	0.44	0.60
Flux ratios (24 h)	β	Q_H/Q_N	Q_E/Q_N	Q_G/Q_N	Resid/Q_N
Average (ratio)	2.53	0.65	0.27	−0.02	0.1
St. dev. (ratio)	0.66	0.06	0.05	0.05	0.4
Flux ratios (daytime)	β	Q_H/Q_N	Q_E/Q_N	Q_G/Q_N	Resid/Q_N
Average (ratio)	2.90	0.56	0.20	0.22	0.02
St. dev. (ratio)	0.71	0.03	0.03	0.03	0.02

4. Conclusions

Observations of surface radiation budget, energy balance and atmospheric surface layer meteorology were made in central Iran in the late summer of 2006. The study area was planted with a desert shrub (*Haloxylon aphyllum*) in order to stabilize dunes encroaching on an urban area. The objectives were to characterize surface-atmosphere exchanges of energy and water, to determine the energy flux partitioning and to compare the surface energy balance with other arid studies as well as aspects of general energy balance theory. The study period was characterized by a strong high pressure system with no clouds or precipitation, warm temperatures and low humidity, typical of the broader region in summer. The following bullet points characterize the main findings of the study.

- Lack of clouds and high solar declination produced strong incident solar radiation, although high atmospheric aerosol concentrations was important for attenuating solar radiation and producing very high atmospheric longwave emission and emissivity compared with 'clear sky' conditions elsewhere.
- A high surface albedo (0.265) and large surface longwave radiation loss produced a low $Q_N/K\downarrow$ as found in other arid studies.
- Partitioning of Q_N was dominated by Q_H and Q_G, which showed strong diurnal asymmetry, with Q_G dominating morning hours and Q_H afternoon. This was only partially explained by empirical models previously considered broadly applicable, and the difference seemed to be governed by changing rates of eddy diffusivity through the day.
- The Bowen ratio was 2.53 over the 24 h period and 2.9 during daylight hours, values that fell within the range of other vegetated arid surfaces.
- Surface temperature gradients were very strong both in the atmospheric surface layer and in the 10 cm beneath the surface, with consistent lapse conditions by day and inversions at night.
- The wind regime was characterized by a strong daytime regional wind system ($\sim 5\ m\ s^{-1}$) which underwent approximately 45° Coriolis turning over a 12 h period and weaker nocturnal slope flows ($\sim 2\ m\ s^{-1}$).
- Actual evapotranspiration ($1\ mm\ dy^{-1}$) was only a small fraction (13.5%) of potential evapotranspiration which showed a very high atmospheric demand and strong surface resistance to water loss. AET increased soon after sunrise, but flattened out at about $0.1\ mm\ h^{-1}$ for the morning before diminishing in the afternoon. This pattern correlates with previous diurnal observations of stomatal conductance in *Haloxylon aphyllum* and shows strong biophysical response to water stress by the vegetation.
- The planting of vegetation for dune stabilization appears to have had a measureable impact on the surface microclimate by providing small but significant atmospheric water and reducing sensible heat flux, which could be as much as 40% larger without the vegetation.

Acknowledgements

This research was supported by a grant from the Department of Geography, University of Canterbury. We would also like to thank our colleagues at the Yazd institute of the Environment (Moheetezist) where the measurements took place. Also thanks to Nick Key for technical assistance and Marney Brosnan for cartographic support, both from the Department of Geography at Canterbury.

References

Baghestani Maybodi, N., Baghestani Maybodi, M.A., Soufizadeh, S., 2006. Pruning height and its effect on quantitative seed production in old saxaul (*Haloxylon aphyllum*) forests of Yazd, Iran. BIABAN Journal 11, 27–33.

Beringer, J., Tapper, N.J., 2000. The influence of subtropical cold fronts on the surface energy balance of a semi-arid site. Journal of Arid Environments 44, 437–450.

Brutsaert, W., 1975. On a derivable formula for long-wave radiation from clear skies. Water Resources Research 11, 742–744.

Campbell, G.S., Tanner, B.D., 1985. A krypton hygrometer for measurement of atmospheric water vapor concentration. In: Eddy Correlation Instrumentation (Models KH20 and CA27), Collected Papers, Version I. Campbell Scientific, Logan, UT.

Cleugh, H.A., Roberts, T., 1994. Local-scale energy balances and microclimate in the desert ranges of central Australia. Australian Meteorological Magazine 43, 219–228.

Foken, T., 2008. The energy balance closure problem: an overview. Ecological Applications 18, 1351–1367.

Grunwald, J., Kalthoff, N., Corsmeier, U., Fiedler, F., 1996. Comparison of areally averaged turbulent fluxes over non-homogeneous terrain. Boundary Layer Meteorology 77, 105–134.

Heusinkveld, B.G., Jacobs, A.F.G., Holtslag, A.A.M., Berkowicz, S.M., 2004. Surface energy balance closure in an arid region: role of soil heat flux. Agricultural and Forest Meteorology 122, 21–37.

Hossenzadeh, S.R., 1997. One hundred and twenty days winds of Sistan. The Iranian Journal of Research in Geography (in Farsi) 46, 103–127.

IPCC, 2007. Climate change 2007: impacts, adaptation and vulnerability. In: Parry, M.L., Canziani, O.F., Palutikof, J.P., van der Linden, P.J., Hanson, C.E. (Eds.), Contribution of Working Group II to the Fourth Assessment Report of the Intergovernmental Panel on Climate Change. Cambridge University Press, Cambridge, UK, p. 976.

Jensen, M.E., Burman, R.D., Allen, R.G. (Eds.), 1990. Evaporation and irrigation water requirements. SCE Manuals and Reports on Eng. Practices No. 70. American Society of Civil Engineering, NY, p. 360.

Kalthoff, N., Fiebig-Wittmaack, M., Mei[ss]ner, C., Kohler, M., Uriarte, M., Bischoff-Gau [ss], I., Gonzales, E., 2006. The energy balance, evapo-transpiration and nocturnal dew deposition of an arid valley in the Andes. Journal of Arid Environments 65, 420–443.

Kampf, S.K., Tyler, S.W., Ortiz, C.A., Munoz, J.F., Adkins, P.L., 2005. Evaporation and land surface energy budget at the Salar de Atacama, Northern Chile. Journal of Hydrology 310, 236–252.

Kustas, W.P., Prueger, J.H., Hatfield, J.L., Ramalingam, K., Hipps, L.E., 2000. Variability in soil heat flux from a mesquite dune site. Agriculture and Forest Meteorology 103, 249–264.

Kobayashi, T., Morimura, A., Temirbekov, S., Morimoto, Y., 2010. Ecofunctional analysis of dryland vegetation: structure, mechanism and their changes. Symposium on the Aral Sea and the surrounding region - Irrigated Agriculture and the Environment. United Nations Environmental Program, Division of Technology, Industry and Economics, Technical Publication 4. http://www.unep.or.jp/ietc/Publications/techpublications/TechPub-4/ecof2-8.asp last accessed June 17, 2010.

Laymon, C., Quattrochi, D., 2004. Estimating spatially-distributed surface fluxes in a semi-arid Great-Basin Desert using Landsat TM data. In: Quattrochi, D., Luvall, J. (Eds.), Thermal Remote Sensing in Land Surface Processes. Taylor and Francis, London, pp. 133–159.

Leuning, R., 2004. Measurements of trace gas fluxes in the atmosphere using eddy covariance: WPL corrections revisited. In: Lee, X., Massman, W., Law, B. (Eds.), Handbook of Micrometeorology. Springer, New York, pp. 119–132.

Malek, E., Bingham, G.E., 1997. Partitioning of radiation and energy balance components in an inhomogeneous desert valley. Journal of Arid Environments 37, 193–207.

Malek, E., Bingham, G.E., McCurdy, G.D., 1990. Evapotranspiration from the margin and moist playa of a closed desert valley. Journal of Hydrology 120, 15–34.

McCaughey, J.H., Saxton, W.L., 1988. Energy balance storage terms in a mixed forest. Agriculture and Forest Meteorology 44, 1–18.

Oke, T.R., 1987. Boundary Layer Climates, second ed. Routledge, New York. 435pp.

Oliphant, A.J., 2000. Spatial and temporal variability of surface energy fluxes in an alpine catchment. Unpublished Ph.D. Thesis, University of Canterbury, Christchurch, New Zealand, 197pp.

Oliphant, A.J., Grimmond, C.S.B., Zutter, H.N., Schmid, H.-P., Su, H.-B., Scott, S.L., Offerle, B., Randolph, J.C., Ehman, J., 2004. Heat storage and energy balance fluxes for a temperate deciduous forest. Agriculture and Forest Meteorology 126, 185–201.

Oliphant, A.J., Hindmarsh, R., Lawson, W., April 2007. Energy and Moisture Fluxes Over and Within Frozen Debris in Polar Conditions: Evidence From The Taylor Valley, Antarctica. European Geosciences Union Annual Meeting, Vienna, Austria.

Oliphant, A.J., Spronken-Smith, R.A., Sturman, A.P., 2003. Spatial variability of surface radiation fluxes in mountainous terrain. Journal of Applied Meteorology 42, 113–128.

Orlovsky, N., Birnbaum, E., 2002. The role of *Haloxylon* species for combating desertification in Central Asia. Plant Biosystems 136, 233–240.

Prater, M.R., DeLucia, E.H., 2006. Non-native grasses alter evapotranspiration and energy balance in Great Basin sagebrush communities. Agriculture and Forest Meteorology 139, 154–163.

Reynolds, J.F., Stafford Smith, D.M., Lambin, E.F., Turner, B.L., Mortimore, M., Batterbury, S.P.J., Downing, T.E., Dowlatabadi, H., Fernández, R.J., Herrick, J.E., Huber-Sannwald, E., Jiang, H., Leemans, R., Lynam, T., Maestre, F.T., Ayarza, M., Walker, B., 2007. Global desertification: building a science for dryland development. Science 316, 847–851.

Santanello Jr., J.A., Friedl, M.A., 2003. Diurnal covariation in soil heat flux and net radiation. Journal of Applied Meteorology 42, 851–862.

Sridhar, V., Elliott, R.L., 2002. On the development of a simple downwelling longwave radiation scheme. Agriculture and Forest Meteorology 112, 237–243.

Sturman, A.P., McGowan, H.A., 2009. Observations of dry season surface energy exchanges over a desert clay pan, Queensland, Australia. Journal of Arid Environments 73, 74–81.

Vepraskas, M.J., 1988. Bulk density values diagnostic of restricted root growth in coarse-textured soils. Soil Science Society of America 52, 1117–1121.

Vehrencamp, J.E., 1952. Experimental investigation of heat transfer at an air–earth interface. Transactions American Geophysical Union 34, 22–30.

Whiteman, C.D.., 1990. Observations of thermally developed wind systems in mountainous terrain, in: Blumen, W.. (Ed.), Atmospheric Processes Over Complex Terrain, Meteorological Monographs, 23 (no. 45), American Meteorological Society, Boston, Massachusetts, 5–42.

Wilson, K., Goldstein, A., Falge, E., Aubinet, M., Baldocchi, D., Berbigier, P., Bernhofer, C., Ceulenmans, R., Dolman, H., Field, C., Grelle, A., Ibrom, A., Law, B.E., Kowalski, A., Meyers, T., Moncrieff, J., Monson, R., Oechel, W., Tenhunen, J., Valentini, R., Verma, S., 2002. Energy balance closure at FLUXNET sites. Agriculture and Forest Meteorology 113, 223–243.

Zawar-Reza, P., 2008. Numerical analysis of the '120 day wind' over the Sistan Region, South-West Asia with TAPM. Clean Environmental Quality 42, 21–24.